DISCRETE STOCHASTIC MODEL FOR THE GENERATION OF AXONAL TREES

Alejandro Mottini[1], Xavier Descombes[1], Florence Besse[2] and Eugene Pechersky[3]

***Abstract*— In this work we propose a 2D discrete stochastic model for the simulation of axonal biogenesis. The model is defined by a third order Markov Chain. The model considers two main processes: the growth process that models the elongation and shape of the neurites and the bifurcation process that models the generation of branches. The growth process depends, among other variables, on the external attraction field generated by a chemoattractant molecule secreted by the target area. We propose an estimation scheme of the involved parameters from real fluorescent confocal microscopy images of single neurons within intact adult *Drosophila* fly brains. Both normal neurons and neurons in which certain genes were inactivated have been considered (two mutations). In total, 53 images (18 normal, 21 type 1 mutant and 14 type 2 mutant) were used. The model parameters allow us to describe pathological characteristics of the mutated populations.**

I. INTRODUCTION

Much effort has been devoted to the morphological analysis of axonal trees. It is known that their morphology impacts network connectivity, thus influencing its functioning. However, many of the mechanisms involved in their morphogenesis are still not completely understood. Therefore, a simulation framework for realistic axonal trees could provide an insight into this process.

Several methods are currently present in the literature, which differ with respect to the processes being modeled, the methodology and type of data used for the parameter estimation and the dimension considered (2D, 3D or 4D).

In [1] the authors introduce a 2D model of self wiring neural networks inspired from previous work on the study of patterning of bacterial colonies. Neurons are represented as being composed of the soma, dendrites and axons. Neurites and somas communicate with each other by means of attractive or repulsive signals that determine the networks morphology.

On the other hand, [2] presents a 3D stochastic model of neuronal growth cones (tips of the growing axon) that takes into account the concentration of guidance molecules to determine their behavior. Although this model presents an interesting approach, the authors do not use the model to estimate the attraction field. Instead, it is an input necessary to simulate the behavior of the axons. Moreover, they do not consider bifurcations.

Finally, Koene et al. [3] propose a very complete model for the generation of 4D (3D and time) neuronal networks that includes both axons and dendrites. For each neurite's growth cone, the model considers the processes of elongation, turning and branching. However, no attraction field is considered. The authors estimate some of the parameters from real 4D data, and others are set manually based on properties of real neurons.

In this paper we propose a 2D discrete stochastic model for the simulation of axonal biogenesis. The model is defined by a three step Markov Random Chain. It considers an external attraction field, and all the involved parameters (including those defining the attraction field) are estimated from real data.

II. MODEL DESCRIPTION

We consider a discrete stochastic process to model the axonal tree formation that considers growth and bifurcation. The growth process models the elongation and shape of the neurites, and depends on both the internal rigidity of the neurite and on an external attraction field. On the other hand, the bifurcation process models the generation of branches. Both processes are considered to be independent from each other. Each branch of the resulting axonal tree is then a realization of a third-order Markov chain.

A. Growth Process

This process models the formation of the neurites on a discrete lattice $L \subset \mathbb{Z}^2$. The number of points N on a filament (i.e. its length) is determined using a Gaussian distribution function $\mathcal{N}(\mu, \sigma^2)$, where μ, σ^2 are parameters to be estimated. This choice was made after fitting different distributions to the lengths observed in our database.

The shape of the path is determined point by point using a second order Markov Chain that depends on the elastic properties of the neurites and on the external attraction field generated by a chemo-attractant molecule secreted by the target area. Given a point n_t on a path, the position of the next point on the path (n_{t+1}) depends on the two previous points n_{t-1}, n_{t-2} and on the external field in n_t ($\Delta(n_t)$). Two main cases are defined (plus all the possible rotations) depending on the configuration of n_t, n_{t-1}, n_{t-2}. For each case, the elasticity contribution is defined on Figure 1. The attraction field is given by the vector $\Delta(n_t) = (\Delta_R(n_t), \Delta_T(n_t))$. Δ_R is the attraction to the right and Δ_T

Alejandro Mottini, Xavier Descombes and Florence Besse are part of Project Morpheme, INRIA/I3S/IBV, Sophia Antipolis, France

[1]INRIA CRI-SAM, 2004 route des Lucioles, 06902 Sophia Antipolis Cedex, France

[2]IBV, Faculté des Sciences, Parc Valrose 06108 Nice Cedex 2, France

[3]A. A. Kharkevich Institute for Information Transmission Problems, Russian Academy of Sciences, Russia.

E. Pechersky work was supported by the RFBR Foundation (grant 14-01-00379). This work was partially supported by the French Government (National Research Agency, ANR) through the "Investments for the Future" LABEX SIGNALIFE : program reference ANR-11-LABX-0028-01

978-1-4244-7929-0/14/$26.00 ©2014 IEEE

to the top of the image (see Figure 4), which are assumed to be positive.

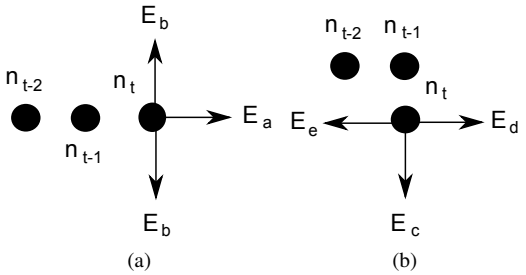

Fig. 1: Diagram showing the two possible main configurations and the different elasticities considered in each case.

To compute the conditional probabilities, we consider the sum of the elasticity and the external field and normalize it. Let us consider the cases presented on Figure 1, and define the following quantities:

$$\begin{cases} S_1 = E_a + 2E_b + \Delta_R(n_t) + \Delta_T(n_t) \\ S_2 = E_c + E_d + E_e + \Delta_R(n_t) + \Delta_T(n_t) \end{cases} \quad (1)$$

Then, the conditional probabilities for n_{t+1} are summarized on Figure 2.

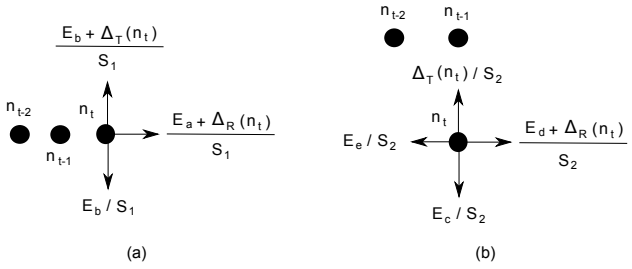

Fig. 2: Conditional probabilities $P(n_{t+1}|n_t, n_{t-1}, n_{t-2})$ associated with the cases presented on Figure 1

The configurations obtained by the possible rotations are treated in a similar way.

B. Bifurcation Process

The bifurcation process is defined by the probability of branching P_b. For a given point n_t in a path, the probability of a branching event taking place in that point is determined by $P_b(n_t)$. This probability is piecewise constant during time.

Branches grow independently of the main axon following the same model.

C. Parameter Estimation

The model parameters are given by $(P_b, \mu, \sigma^2, E_a, E_b, E_c, E_d, E_e)$ and the external field $(\Delta_x(u,v), \Delta_y(u,v))$, for $(u,v) \in L$.

Let us consider a set of axonal trees $\mathbb{A}$ (where $\mathbb{A}$ could be equal to 1), Denote by l_a, $a \in \mathbb{A}$ the length (i.e., number of pixels) of the main branch of axon a. We then have:

$$\hat{P_b} = \frac{\sum_{a \in A} N_b(a)}{\sum_a l_a} \quad (2)$$

where $N_b(a)$ is the number of branches in a.

Moreover, the mean and variance of the probability distribution that determines the length of a path is equal to μ and σ^2. Therefore, we have the following estimators:

$$\hat{\mu} = \frac{\sum_{a \in \mathbb{A}} l_a}{card(A)} \qquad \hat{\sigma^2} = \frac{\sum_{a \in \mathbb{A}} (l_a - \hat{\mu})^2}{card(A)} \quad (3)$$

For the remaining parameters, we assume that Δ is constant. As we will see in section III, Δ can be approximated as being constant over subsets of L. Notice also that if we consider several axons, they all need to be registered in the same space.

There remains seven parameters. For each configuration of the past (i.e, n_{t-1}, n_{t-2})) we obtain three or four equations depending on which case we are on (see Figure 2). This gives forty eight equation in total when we take into account all the possible rotations. If we consider the cases associated to configuration (a) in Figure 2, we obtain the following three equations:

$$\begin{cases} \frac{N_1}{N_T} = \frac{\hat{E_a} + \hat{\Delta_R}}{\hat{S_1}} \\ \frac{N_2}{N_T} = \frac{\hat{E_b} + \hat{\Delta_T}}{\hat{S_1}} \\ \frac{N_3}{N_T} = \frac{\hat{E_b}}{\hat{S_1}} \end{cases} \quad (4)$$

where $N_{1,2,3}$ are the number of times that the configurations given on Figures 3 (a, b, c) are present on the axon, $N_T = N_1 + N_2 + N_3$ and $\hat{S_1} = \hat{E_a} + 2\hat{E_b} + \hat{\Delta_R} + \hat{\Delta_T}$.

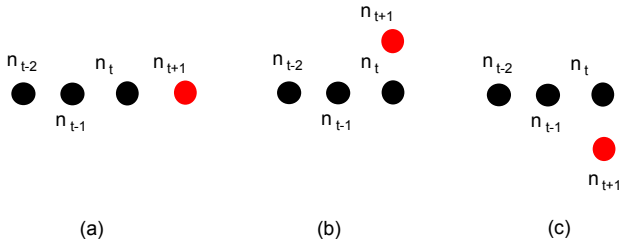

Fig. 3: The 3 possible positions of n_{t+1} for the configuration present in Figure 2 (a).

Thus, we obtain the following linear equations:

$$\begin{cases} (\frac{N_1}{N_T} - 1).\hat{E_a} + 2.\frac{N_1}{N_T}.\hat{E_b} + (\frac{N_1}{N_T} - 1).\hat{\Delta_R} + \frac{N_1}{N_T}.\hat{\Delta_T} = 0 \\ \frac{N_2}{N_T}.\hat{E_a} + (2.\frac{N_2}{N_T} - 1).\hat{E_b} + \frac{N_2}{N_T}.\hat{\Delta_R} + (\frac{N_2}{N_T} - 1).\hat{\Delta_T} = 0 \\ \frac{N_3}{N_T}.\hat{E_a} + (2.\frac{N_3}{N_T} - 1).\hat{E_b} + \frac{N_3}{N_T}.\hat{\Delta_R} + \frac{N_3}{N_T}.\hat{\Delta_T} = 0 \end{cases} \quad (5)$$

The same reasoning is applied to obtain the total system of forty eight equations, which we solve using the Least Mean Squared (LMS) method.

In a real scenario, we would expect the values of the probabilities to change depending on the position of the considered point. This is particularly true for the attraction field, since the sensitivity to attractive gradients varies along the gradient and gets lower close to the source present at the upper edge of each image (see Section III). Therefore, we calculate the values of the probabilities for each point of a path using a sliding window scheme. The optimum size of the estimation window was calculated by first using

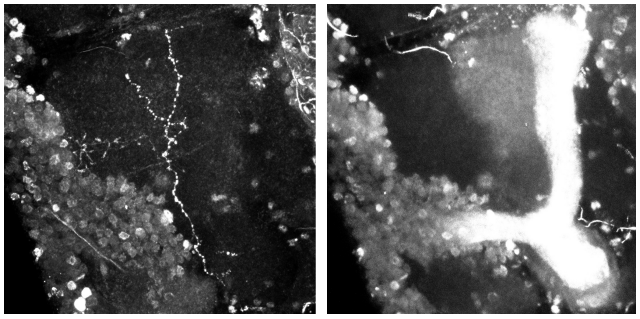

Fig. 4: Channel 1 (left; GFP staining) and 2 (right; Fasciclin II staining) for a given image (maximum intensity projections).

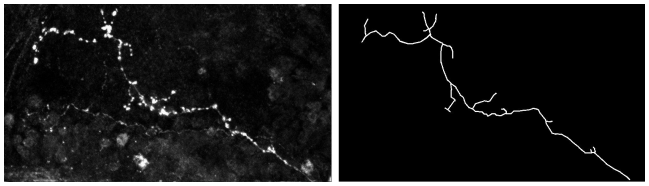

Fig. 5: Original confocal microscopy image of an axonal tree (left) and its tracing (right) (maximum intensity projections).

the model to simulate paths with known probabilities, and then running the estimation procedure using different sizes of windows and calculating the error between the two. We determined that a good compromise between error of the estimation and size of the window is 800 points.

III. VALIDATION

For the validation, we have fluorescently labeled single neurons within intact adult *Drosophila* fly brains, and have acquired 3D fluorescent confocal microscopy images of their axonal trees. Both normal neurons and neurons in which the function of the *imp* (mutant type 1) or *profilin* (mutant type 2) genes was inactivated were imaged. *imp* encodes a conserved RNA binding protein controlling subcellular mRNA transport and local protein synthesis, and is essential for axonal remodeling [4]. *profilin* encodes a regulator of the actin cytoskeleton involved in axonal pathfinding [5]. Mutations in these two conserved genes have been linked to neurological pathologies [6], [7].

Each image stack has a resolution of $0.093967 \times 0.093967 \times 0.814067\ \mu m$ and two channels (see Figure 4). The morphology of single axonal trees is visible in the first channel and was manually segmented by an experienced biologist (see Figure 5). The morphology of the overall neuronal structure in which axons are developing is visible in the second channel. In total, 53 images (18 normal, 21 type 1 mutant and 14 type 2 mutant) were used.

In order to study the attraction field of the populations, all stacks were registered against the first image of the normal population. This was performed using the second channel of each images, and the transformations were then used to correct the first channel. Images were registered by first aligning them with a rigid registration algorithm, followed by a non linear demons registration step.

Due to the ratio between the resolution on the z axis and on the x,y plane, we have considered the maximum intensity projections of the images along the z axis.

A. Results

We have estimated the model parameters for each hierarchical level of each image, and then averaged these values between the images to obtain sets of representative values for each population. We have used these values to generate several axonal trees for each population to visually compare the obtained simulations with the real images (see Figure 6). We determine that the real and synthetic images present a similar morphology.

Moreover, given that all images were registered, we are able to use the estimated parameters to generate two fields for each population, a scalar field that represents the magnitude of E_a/E_b and a vector field that represents the attraction field Δ. Since we obtain some estimates on a sparse set of points in the x,y plane, we extrapolate the fields using a Gaussian Markov Random Field [8].

In addition, we have averaged the second channel of all the registered images to obtain an approximation of the average shape of the overall neuronal structure in which axons are developing. We have then plotted the Δ field for each population on these three mean images. By qualitatively analyzing the resulting images we have determined that there is no relevant difference on the field between the three populations (see Figure 7, we only present the results for the normal populations because they are very similar with respect to the other populations). We can appreciate that the field points towards the target area (which is located at the top right corner of the image) and that its norm is stronger at the starting point of the axons (bottom right section) and weaker near the target area.

The same procedure was used to analyze the difference on the scalar fields for each population (see Figure 8). In this case we can detect a significant difference between the populations. Given that E_a/E_b is related to the flexibility of the axons, we can determine that the normal axons have a more constant direction throughout its length, followed by mutant type 2 and mutant type 1 (see Figure 8).

IV. CONCLUSIONS

In this paper we propose a 2D discrete stochastic model for the simulation of axonal trees based on Markov Chains. The model considers several independent processes (elongation, shape and bifurcation) that are determined by several parameters, all of which can be directly estimated from real static data. We have validated the model on a set of 53 real fluorescent confocal microscopy images of single neurons within intact adult *Drosophila* fly brains. Both normal neurons and neurons in which certain genes were inactivated were considered (18 normal, 21 mutant type 1 and 14 type 2). For each class of neurons, we have estimated the parameters

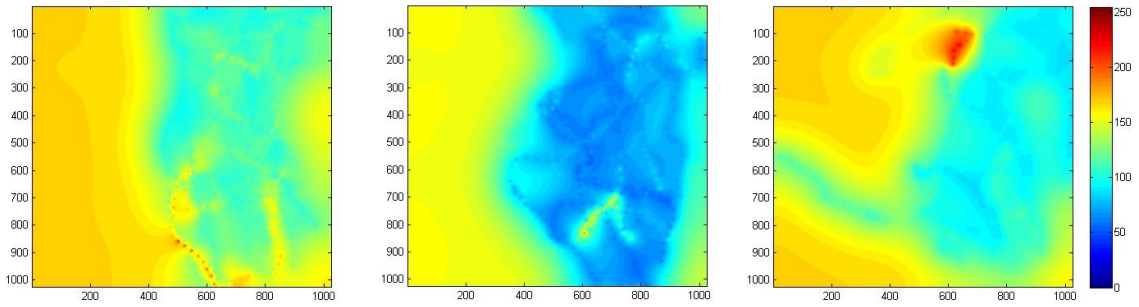

Fig. 8: E_a/E_b scalar field for the normal (left), mutant type 1 (middle) and mutant type 2 (right) populations.

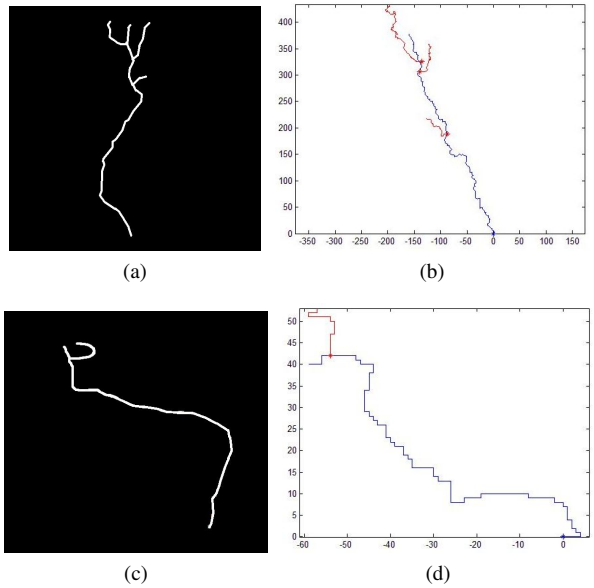

Fig. 6: Real normal and mutant type 1 axonal trees (left top and bottom respectively) and synthetic trees (right, top and bottom) generated using the parameters estimated from each respective image.

and generated synthetic axonal trees, which are similar to the real ones. Moreover, results show that the parameter's values provide information about the axon growth properties of the populations. In the future we intend to extend the model to 3D and to include the growth speed by considering 3D time sequences of developing axons.

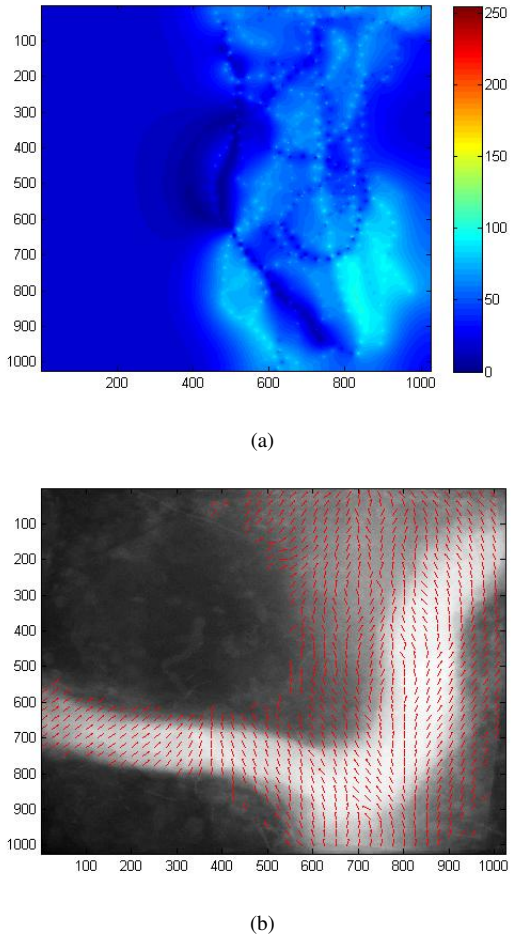

Fig. 7: Norm (top) and direction (bottom) of the attraction field for the normal population.

REFERENCES

[1] Segev R., Ben-Jacob E. Generic modeling of chemotactic based self-wiring of neural networks. *Neural Networks*, Mar;13(2):185-99, 2000.

[2] Kobayashi T., Terajima K., Nozumi M., Igarashi M., Akazawa K. A stochastic model of neuronal growth cone guidance regulated by multiple sensors. *Journal of Theoretical Biology*, 21;266(4):712-22, 2010.

[3] Koene R.A., Tijms B., van Hees P., Postma F., de Ridder A., Ramakers G.J.A. , van Pelt J., van Ooyen A. NETMORPH: A Framework for the Stochastic Generation of Large Scale Neuronal Networks With Realistic Neuron Morphologies. *Neuroinformatics*, Volume 7, Issue 3, pp 195-210, September 2009.

[4] Medioni C., Ramialison M., Ephrussi A., Besse, F. Imp promotes axonal remodeling by regulating profilin mRNA during Drosophila brain development. *In press, Current Biology*.

[5] Wills Z., Marr L., Zinn K., Goodman C.S, Van Vactor D. Profilin and the Abl tyrosine kinase are required for motor axon outgrowth in the Drosophila embryo. *Neuron*, 22, 291−299, 1999.

[6] Donnelly C.J. et al. Limited availability of ZBP1 restricts axonal mRNA localization and nerve regeneration capacity. *EMBO J*, 30(22):4665−77, 2011.

[7] Wu C.H. et al. Mutations in the profilin 1 gene cause familial amyotrophic lateral sclerosis. *Nature*, 488(7412):499−503, 2012.

[8] Winkler G. Image Analysis, Random Fields and Markov Chain Monte Carlo Methods: A Mathematical Introduction (Stochastic Modelling and Applied Probability). *Springer*, ISBN-10: 3540442138.